The Astrophysical Journal, 698:1000–1009, 2009 June 20 doi:10.1088/0004-637X/698/2/1000

COMPARISON AMONG Ca II K SPECTROHELIOGRAM TIME SERIES WITH AN APPLICATION TO SOLAR ACTIVITY STUDIES

I. Ermolli[1], S. K. Solanki[2], A. G. Tlatov[3], N. A. Krivova[2], R. K. Ulrich[4], and J. Singh[5]
[1] INAF, Osservatorio Astronomico di Roma, Via Frascati 33, 00040 Monte Porzio Catone, Italy; ermolli@oaroma.inaf.it
[2] Max-Planck-Institut für Sonnensystemforshung, Max-Planck-Strasse 2, 37191 Katlenburg-Lindau, Germany
[3] Kislovodsk Solar Station, Pulkovo Observatory, Pulkovskoe Ch. 65-1, 196140 Saint Petersburg, Russia
[4] Division of Astronomy and Astrophysics, University of California, 8371 Mathematical Science Building, Los Angeles, CA 90095-1562, USA
[5] Indian Institute of Astrophysics, 2nd Block, Koramangala, 560034 Bangalore, India
Received 2008 February 28; accepted 2009 March 25; published 2009 May 27

ABSTRACT

Various observatories around the globe started regular full-disk imaging of the solar atmosphere in the Ca II K line in the early decades of the 20th century. The archives made by these observations have the potential of providing far more detailed information on solar magnetism than just the sunspot number and area records to which most studies of solar activity and irradiance changes are restricted. We evaluate the image quality and contents of three Ca II K spectroheliogram time series, specifically those obtained by the digitization of the Arcetri, Kodaikanal, and Mt Wilson photographic archives, in order to estimate their value for studies focusing on timescales longer than the solar cycle. We analyze the quality of these data and compare the results obtained with those achieved for similar present-day observations taken with the Meudon spectroheliograph and with the Rome-PSPT. We also investigate whether image-segmentation techniques, such as those developed for identification of plage regions on present-day Ca II K observations, can be used to process historic series. We show that historic data suffer from stronger geometrical distortions and photometric uncertainties than similar present-day observations. The latter uncertainties mostly originate from the photographic calibration of the original data and from stray-light effects. We also show that the image contents of the three analyzed series vary in time. These variations are probably due to instrument changes and aging of the spectrographs used, as well as changes of the observing programs. The segmentation technique tested in this study gives reasonably consistent results for the three analyzed series after application of a simple photographic calibration. Although the plage areas measured from the three analyzed series differ somewhat, the difference to previously published results is larger.

Key words: methods: data analysis – Sun: activity – Sun: chromosphere – Sun: faculae, plages

Online-only material: color figures

1. INTRODUCTION

A wide variety of solar research, ranging from the investigation of global solar activity and variability to the study of large-scale patterns of proper motions, is based upon the analysis of regular full-disk observations of the Sun. Only during the last 1–2 solar cycles have such observations been carried out by space-based telescopes and by a new generation of ground-based instruments, e.g., by *Yohkoh*/SXT (Acton et al. 1992), *SOHO*/EIT (Delaboudinière et al. 1995), *SOHO*/MDI (Scherrer et al. 1995), PSPT (Coulter & Kuhn 1994; Ermolli et al. 1998), CFDT2-SFO (Chapman et al. 2004), and SOLIS (Keller et al. 2003). These observations are thus of limited usefulness for focusing on timescales longer than the activity cycle. For such studies regular full-disk observations of the solar atmosphere starting at the beginning of the 20th century at several observatories are of particular interest (for a list of synoptic programs carried out before 1950 see Mouradian & Garcia 2007). These historic observations were made in white light and in various spectral bands, often in the Ca II K and Hα resonance lines, mostly using spectroheliographs.

Among the historic series, those including Ca II K observations have the largest potential of providing information about solar magnetism. In fact, Ca II K emission can be used as a good proxy of the line-of-sight magnetic flux density (Skumanich et al. 1975; Schrijver et al. 1989). Note that in standard notation K_3, $K_{2V,2R}$, and $K_{1V,1R}$ mark the core, the reversal (emission peaks), and the secondary minima of the doubly reversed profile of the Ca II K line, in the violet (V) and the red (R) wings of the line, respectively. All these line features occur within a spectral range less than 1 Å wide.

To date extensive analysis of historic Ca II K spectroheliogram time series was restricted for two reasons: (1) lack of data in digital format; (2) shortcomings and defects that beset historic data. The first restriction should be overcome soon by the results of new projects devoted to the digitization and distribution of some of the major photographic archives. For instance, Arcetri, Kodaikanal, and Mt Wilson Ca II K historic observations have recently been digitized (Ulrich et al. 2004; Makarov et al. 2004; Marchei et al. 2006), and other similar series are now being processed as well. Some Ca II K series already underwent digitization and analysis in the 1990s, when selected (regularly spaced) spectroheliograms or almost entire series were converted at $\leqslant 2''$ pixel^{-1} (e.g., Ribes & Mein 1985 (p. 282); Kariyappa & Pap 1996; Caccin et al. 1998; Worden et al. 1998) or $\geqslant 5''$ pixel^{-1} (Foukal 1996) resolution, respectively. Defects in and decay of spectroheliogram photographic plates, missing photographic calibration, and undocumented changes of the instrumentation lead to various artifacts in and problems with the historic data (Zharkova et al. 2003; Fuller et al. 2005; Ermolli et al. 2007), which are avoided in the full-disk images taken by the most recent synoptic observing programs.

Here, we intercompare and discuss three time series of images obtained by the digitization of Ca II K historic spectroheliograms. We describe these data (Section 2) and analyze their

Table 1
Description of the Instrumentation Used to Obtain the Solar Observations Considered in This Study (Top Panel), of the Devices Utilized to Record the Analyzed Images, Either Digitization Device or Detector (Middle Panel), and of the Data Managed in the Following (Bottom Panel)

Time series	Arcetri	Kodaikanal	Mt Wilson	Meudon	PSPT
Acronym	Ar	Ko	MW	Me	PSPT
Period	1931–1974	1907–1999	1915–1985	2004–2006	1998–2008
Instrumentation	Spectrograph	Spectrograph	Spectrograph	Spectrograph	
	Grating	2 prisms	Grating	Prism	Interference
	600 lines mm^{-1}		590 lines mm^{-1}		filter
Ruled area	100 mm × 110 mm		103 mm × 107 mm		
Solar-disk size (mm)	≈65	≈60	≈50	≈65	≈27
Image scale (mm/″)	0.033	0.031	0.026	0.033	0.028
Spectral window (Å)	0.3	0.5	0.2	0.15	2.5
Recording device	Photographic plate	Photographic plate	Photographic plate	CCD camera	CCD camera
Bibliography	1	3	5	7	8
Digitization at	Rome Observatory	Kodaikanal	UCLA	...	...
Used device	Commercial scanner	Linear array	Commercial scanner		
Settings	1200 × 1200 dpi	900 pixels	1200 × 1200 dpi		
Data product	TIFF	JPEG	TIFF	FITS	FITS
Data dimension (pixels)	2040 × 2740	≈1800 × 1800	≈2600 × 2600	1300 × 1300	2048 × 2048
Number of images	5976	26640	≈40000		
Number of observing days	5042	26620	> 22000		
Bibliography	2	4	6	...	...
Format of analyzed data	FITS	JPEG	FITS	FITS	FITS
Data dimension (pixels)	1020 × 1020	1800 × 1800	800 × 800	1300 × 1300	1024 × 1024
Data type	16 bit	8 bit	16 bit	14 bit	16 bit
Pixel scale (″ $pixel^{-1}$)	2.4	1.3	2.7	1.5	2
Number of analyzed images	4052	19522	34166	1044	4448
Number of observing days	3927	19172	> 20640	87	2838
Access to data archive	9	...	10	11	12

Notes. Details are given in Section 2.1. The variation of image size affecting the MW and Ko series is described in Section 2.2.
References. (1) Godoli & Righini 1950, Gasperini et al. 2004, (2) Centrone et al. 2005, Giorgi et al. 2005, Marchei et al. 2006, (3) Evershed 1911, Bappu 1967, (4) Makarov et al. 2004, (5) Ellerman 1919, (6) Ulrich et al. 2004, Lefebvre et al. 2005, (7) Deslandres 1891, Deslandres & D'Azambuja 1913, (8) Coulter & Kuhn 1994, Ermolli et al. 1998.
Access to data archive: (9) http://cvs3.mporzio.astro.it/~cvs/cvs/arcetri.html, (10) http://www.astro.ucla.edu/~ulrich/MW−SPADP/, (11) http://bass2000.obspm.fr, (12) http://www.mporzio.astro.it/solare.

quality. In particular, we measure the image contents through several quantities (Section 3) and compare the results obtained for historic series with those achieved for similar present-day observations. Subsequently, we test the use of the analyzed time series for the modeling of solar activity variations (Section 4). We discuss the obtained results and present our conclusions (Section 5).

2. DATA

2.1. Data Description

The current analysis concentrates mainly on images obtained from the digitization of Ca II K spectroheliograms stored in the photographic archives of the Arcetri (hereafter referred to as Ar), Kodaikanal (Ko hereafter), and Mt Wilson (MW hereafter) Observatories. These data are henceforth collectively referred to as historic data. In addition, we have also analyzed samples of Ca II K images obtained by two current synoptic programs, namely, those carried out with the Meudon spectroheliograph (Me hereafter) and with the Rome-PSPT telescope (PSPT hereafter). These data are henceforth referred to as modern data.

The main characteristics of the instrumentation used to obtain the original photographic data, of the devices utilized for their digitization, and of the images analyzed in this study are summarized in Table 1. Sample images are shown in Figure 1. In addition to the MW data set, described in Table 1, we have also analyzed two other samples of MW images. The first sample contains 237 full-size images taken in the month of July from 1920 to 1930, which are in the form of 16 bit FITS files and have ≈2600 × 2600 pixels each. The analysis of this sample aims at evaluating the sensitivity of the results to the reduction of the image size (Section 3.1). The other analyzed sample contains 8650 reduced-size images (800 × 800 pixels) which were photographically calibrated by scientists at UCLA. These images (MW/UCLA hereafter) were obtained by applying a calibration method based on that presented by de Vaucouleurs (1968) with some modifications. This method makes use of calibrated exposures made on the plates outside the solar disk for the data acquired from late 1961 onward. This sample contains MW observations taken from late 1961 to 1985.

2.2. Data Preprocessing

Flat fielding. The images of all the analyzed series, except for the Ko ones, were independently preprocessed in order to apply the flat-field calibration of the recording device, either digitization device for historic data or detector for modern sets (Centrone et al. 2005; Lefebvre et al. 2005; Ermolli et al. 2003). Visual inspection of images shows that the Ko series lacks such preliminary calibration. However, the measurements considered in this study are only slightly affected by dust accumulation and device defects seen on Ko images.

Solar disk center and radius measurements. Photographic calibration of images and analysis of image contents described in the following require the knowledge of both position of the center and radius of the observed solar disk. For the MW images,

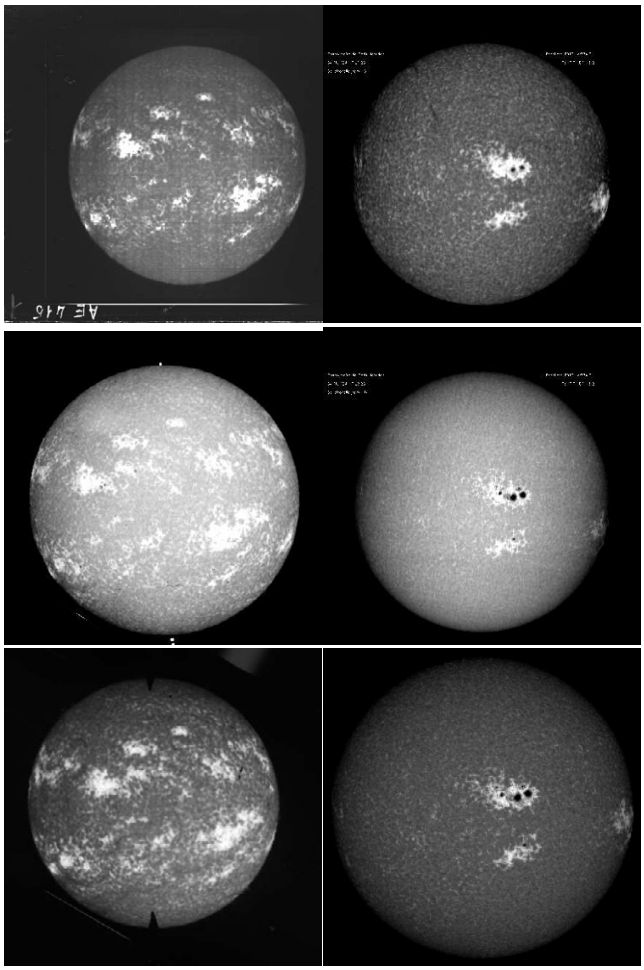

Figure 1. Examples of the Ca II K observations analyzed in this study. Ar (top left), Ko (middle left), and MW (bottom left) historic images obtained by the digitization of spectroheliograms taken at the three sites on 1958 January 9. All these images show sunspots when inspected at full resolution; the MW image (bottom left) clearly also shows on-disk filaments. The Ar image (top left) shows signs of a filament near the right limb (in the lower activity belt). Note that the pixel values were reversed, in order to show the brightness pattern as it is usually observed in intensity images of the solar disk. K_3 (top right) and K_{1V} (middle right) Me spectroheliograms and PSPT filtergram (bottom right) taken at the two sites on 2004 July 24 (≈07:20 UT). All the images were rotated to show heliospheric north on the top.

information about the solar disk center, disk horizontal and vertical radii, and the quality of their measurements is stored in the FITS headers of images. For the other sets (Ar, Ko, Me, and PSPT), the solar disk parameters had to be estimated. We determined the disk center and radius using a method consisting of three steps, partly based on techniques described in the literature (e.g., Walton et al. 1998; Denker et al. 1999; Zharkova et al. 2003). In brief, the method searches for the solar rim, by marking the location of pixels in which two selection criteria are simultaneously fulfilled. The two criteria are: (1) the value of the marked pixel is higher than a given threshold value, which is computed taking into account the mean value of pixels belonging to a subarray centered at the baricenter of pixel values of the image and (2) the gradient of pixel values along the analyzed half-line finds a maximum value at the marked pixel. The position of the marked pixels, i.e., the solar rim is then used for the computation of the disk center and shape, which is performed by applying an ellipse-fitting algorithm. On average, this method gives values of the horizontal and vertical radii of MW solar observations which are about 1.5 pixel smaller than those given in the file headers. This difference corresponds to less than 0.5% of the radius. Note that each historic series analyzed in this study shows specific characteristics and artifacts such that the algorithm for center and radius measurements needs considerable modifications for application to each series.

Data resizing. The image size varies in two of the analyzed historic series, namely, in MW and Ko sets. The size of MW images changes by up to about 4% over the whole series. It is typically larger for the data from 1962 October 8th onward, due to changes that occurred in the spectroheliograph. The size of Ko images for three periods, namely, 1927, 1950–1955, and 1991–1999, is only half of the size of all other Ko data. Ko data during these periods are not included in the comparison of time series presented in Section 3.1. This is meant to ensure that no bias due to the originally different pixel sizes enters the results.

Most of the results presented in the following were obtained by analyzing resized images. This is to guarantee similar solar disk size in all series, and thus to allow their direct comparison. Moreover, this image resizing also helps to compensate for the geometrical distortions affecting some of the analyzed data. In particular, both horizontal and vertical radii of the solar disk were resized to 350 pixels in all images, i.e., roughly to the size of the MW data. By this image resizing, the Ar and Ko data were resampled to about half the linear size of the original digital images. Note that compensation for geometrical distortions improves the accuracy of results provided by the image processing steps required for physical measurements. These steps include, e.g., compensation for the center-to-limb variation of the quiet Sun intensity and identification of bright features for measurements of contrast distributions and of plage areas (see Section 4.1).

Photographic calibration. Values for each pixel (pixel value, PV hereafter) of the Ar, Ko, and MW images were provided by the scanning devices and measure the flux of the scanner beam transmitted through the photographic plate (negative). Given a proper scanner calibration, PV is a measure of the blackening degree of the photographic plate at the position corresponding to that pixel. The blackening is linked to the flux of solar radiation incident during the plate exposure by a relation named the calibration curve. This relation depends on many plate characteristics (Dainty & Shaw 1974).

Since only a small fraction of the analyzed historic images contains calibration exposures, we performed the photographic calibration of all the analyzed data using a method independent of calibration exposures. We converted the image pixel value PV of the Ar, Ko, and MW images into relative calibrated intensity values according to the formula (Mickaelian et al. 2007): $I_i = (V - B)/(T_i - B)$, where I_i is the calibrated intensity (in arbitrary units) of pixel number i, V is the average PV for the unexposed part of the plate, B is the average PV for the darkest, i.e., the most strongly exposed pixels, and T_i is the PV for pixel number i. The pixels of the unexposed part of the plate are identified in each image as those outside the solar disk with PV higher than the maximum PV of solar disk pixels. The darkest pixels in each uncalibrated image are those with PV equal to the minimum PV of solar disk pixels. The effects of modifying the criteria for the identification of darkest and unexposed pixels upon the contents of the analyzed data and the accuracy of the method are discussed in Section 3.2.

The pixel values in the Me and PSPT images were provided by a CCD recording device. Given a proper instrumental calibration, these values are almost linearly proportional to the flux of radiation incident during the exposure of the device.

Table 2
Average Value and Standard Deviation of Measurement Results for the Analyzed Data Sets

	Ar	Ko	MW	Me	PSPT
Solar disk eccentricity	0.14 ± 0.04	0.12 ± 0.06	0.12 ± 0.04	0.14 ± 0.02	0.04 ± 0.03
Spatial resolution resized data	$5\farcs9 \pm 0\farcs2$	$5\farcs9 \pm 0\farcs1$	$6\farcs9 \pm 0\farcs6$	$6\farcs6 \pm 0\farcs4$	$6\farcs5 \pm 0\farcs3$
Spatial resolution full-size data	$5\farcs4 \pm 0\farcs1$	$3\farcs3 \pm 0\farcs1$	$2\farcs6 \pm 0\farcs6$	$4\farcs3 \pm 0\farcs3$	$5\farcs0 \pm 0\farcs4$
Large-scale inhomogeneities	$14\% \pm 18\%$	$12\% \pm 6\%$	$7\% \pm 6\%$	$3.9\% \pm 2.2\%$	$2.2\% \pm 2.2\%$
Stray-light level	0.32 ± 0.15	0.20 ± 0.11	0.48 ± 0.18	0.05 ± 0.03	0.02 ± 0.01
Image contrast	0.7 ± 0.3	0.8 ± 0.2	0.6 ± 0.3	0.53 ± 0.05	0.51 ± 0.04

Note. Details are given in Section 3.1.

Table 3
Standard Deviation of Annual Averages of Measurements Obtained from the Three Historic Series

	Ar	Ko	MW
Solar disk eccentricity (%)	14	32	15
Resolution of resized data (%)	4	3	5
Large-scale inhomogeneities (%)	43	37	96
Stray-light level (%)	25	29	28
Image contrast (%)	23	20	40

Notes. The values are given as percentage fraction of the median value obtained for the analyzed series. Details are given in Section 3.1.

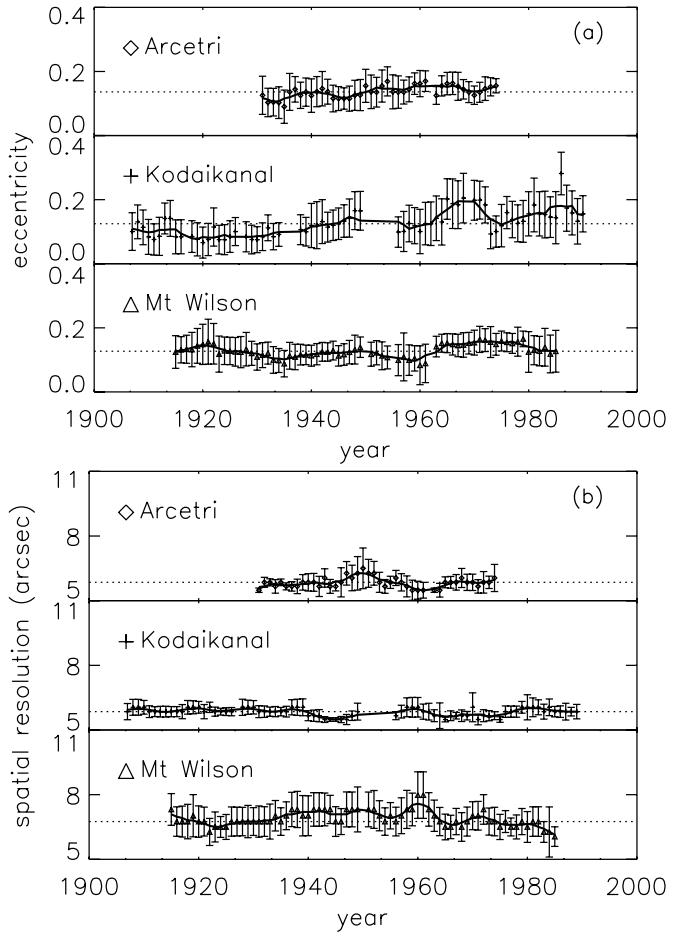

Figure 2. Temporal variation of the solar disk eccentricity (a) and of the spatial scale (b) measured for the Ar, Ko, and MW series. The error bars represent the dispersion of measurements in terms of their standard deviation. The dotted line marks the median value of the average annual results for the whole series. The solid lines represent five year running means.

3. COMPARISON OF TIME SERIES

3.1. Image Quality and Contents of the Time Series

We measured several quantities in each image of the analyzed series, in order to evaluate both data contents and homogeneity in time. In particular, we measured the level of geometrical distortions, of large-scale inhomogeneities, and of stray-light degradations on the images. Furthermore, we measured the spatial resolution and contrast on the solar disk. The results obtained from our measurements are summarized in Tables 2 and 3. Details are given in the following.

Geometrical distortions. We analyzed the parameters of the ellipse which best fits the solar disk edge. We found that Ar and MW series suffer from geometrical distortions, which are predominantly in the horizontal and vertical directions. In contrast, the orientation of the best-fit major and minor axes of the ellipse to Ko images rotates depending on the image. We determine the solar disk eccentricity $e = \sqrt{1 - (r_{\min}/r_{\max})^2}$, where $r_{\min}$ and $r_{\max}$ are the smallest and the largest radii of the solar image.

We found (Table 2) that disk eccentricity of both historic (Ar, Ko, and MW) and modern (Me) spectroheliogram observations is about three times larger than that computed for modern observations taken with interference filters (PSPT). Besides, we found a slight continuous increase of disk eccentricity in the Ar series and a marked increase of the dispersion of results obtained for the Ko data taken from about 1960 onward (Figure 2(a), Table 3). The latter is mostly due to a marked decrease of the image quality and a subsequent increase of failures in the ellipse-fitting calculations. In contrast, the geometrical distortion of solar disk observations on MW data remains almost constant over the whole series. The measured value slightly increases for the data taken from 1962 onward.

Spatial resolution of resized images. We studied power spectra of a 64×64 subarray extracted at the solar disk center. In particular, for each image we measured the spatial frequency at which 98% of the image power spectral density is taken into account. The bulk of the information about patterns in the images lies at frequencies below this. The spatial scale corresponding to this measured cutoff frequency is taken as a measure of the spatial resolution in the analyzed image. Since results are affected by the image defects, we did not employ the usual technique of noting the spatial frequency at which the power drops to the noise level. The usage of a small subarray and of the 98% threshold is also aimed to avoid the detection of power associated with the occurrence of solar activity features and image defects, respectively. The spatial resolution of the historic series is plotted in Figure 2(b). We found that, on average, Ar and Ko images appear to carry more spatial information than the MW data, although the difference is rather small (see Table 2). This result can partly be explained by

the differences in the spectral sampling of the analyzed series. In fact, the nominal narrower spectral sampling of MW data with respect to the other historic series corresponds to observations of higher atmospheric levels compared with the others, and thus to observed features characterized by lower spatial details. This holds also for modern Me images with respect to the PSPT ones.

We also found that the spatial scale of all the three historic series slightly varies in time (Figure 2(b), Table 3). In particular, the spatial resolution on the MW images steadily increased after 1960. This variation is likely due to instrumental changes (e.g., differences in the spectral sampling of the data). Note that the variation of image size affecting the MW data also contributes to the increase of the spatial resolution measured for MW images from 1960 onward. However, the measured resolution increase is about 20% larger than that expected by taking into account the variation of the solar disk size in the analyzed images. Finally, our results suggest that the spatial resolution of the Ko data varies over the whole period less than for the other sets, lying generally close to the one limited by the spatial sampling of analyzed data.

Spatial resolution of full-size images. We found that the average spatial resolution measured on Ar, Ko, and MW full-size images is close to that limited by the spatial sampling of the analyzed data. Moreover, the values of the average resolution measured at the solar disk center and outside the solar disk are within one standard deviation in measurements. These results suggest that the power density found at the smallest spatial scales in the full-size data depends on image digitization. We then resized the images using linear interpolation to half, one-third, and one-fourth the original dimension and analyzed their resolution at the disk center. In particular, we analyzed the distributions of measured values and computed the moments of these distributions. The obtained values indicate that the images can be resized to roughly half the original dimension without loss of solar information. A further reduction in size, however, implies a loss of spatial information on solar features.

Large-scale inhomogeneities. We evaluated the level of large-scale inhomogeneities in the images introduced by variations of the sky transparency during observations and by instrumental problems. In particular, we analyzed the median intensity over a ring centered on the solar disk center of each image and spanning the disk positions $\mu = 0.50 \pm 0.05$. Since strong inhomogeneities could possibly affect only a portion of the solar image, we divided the solar disk into four quadrants and calculated the deviation of the median intensity value in each quadrant, with respect to the median value over the whole ring. We then took the maximum deviation measured over the four quadrants as a measure of the degree of large-scale intensity inhomogeneities affecting the solar disk images. This quantity is plotted in Figure 3(a) for the three historic series. Note that the usage of median intensity values and of the disk positions $\mu = 0.50 \pm 0.05$ is aimed to lower the influence of active regions on the obtained results.

We found that the level of large-scale inhomogeneities affecting historic observations (Ar, Ko, and MW) is higher than that influencing present-day data (Me and PSPT), although the level obtained for MW data is comparable to that obtained for similar current data (Me). Furthermore, we found that the first half of the Ar series, as well the MW data taken during the first decade of observation, suffer from strong large-scale inhomogeneities (Figure 3(a), Table 3). Indeed, Ar and MW logbooks report that image vignetting was very strong at

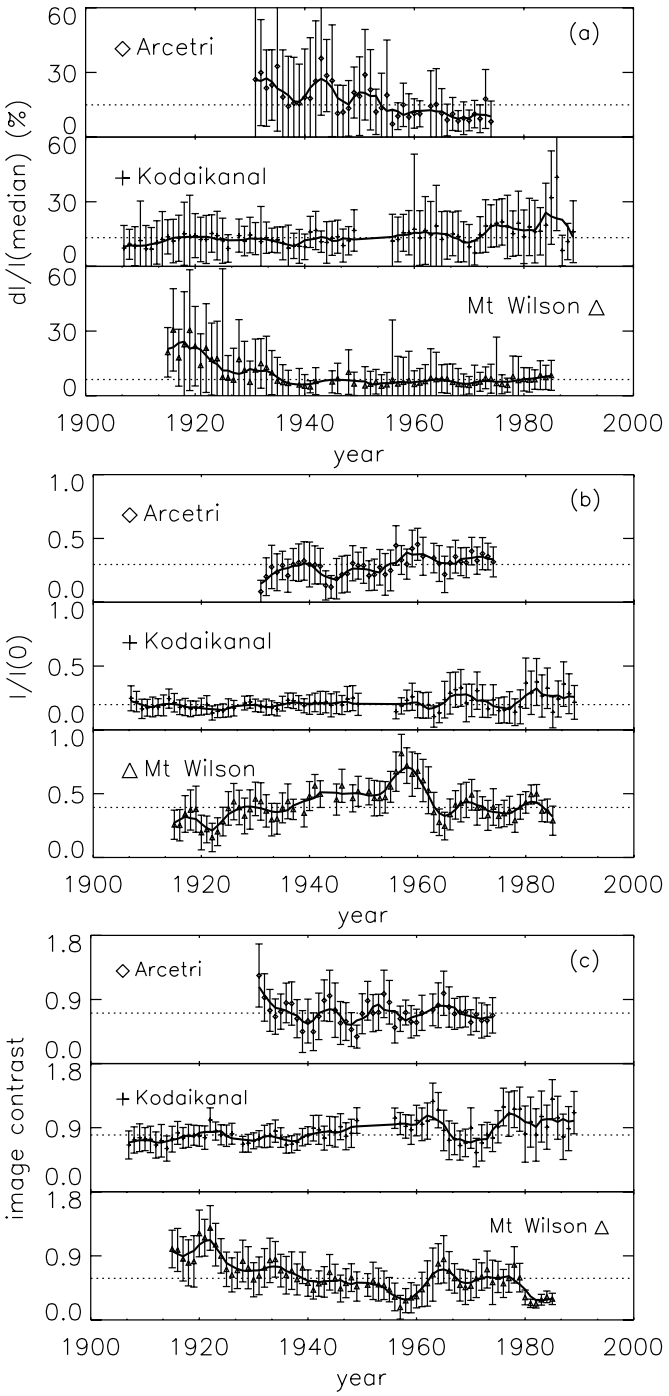

Figure 3. Temporal variation of the large-scale inhomogeneities (a), of the level of stray light evaluated at $r/R_\odot = 1.06 \pm 0.01$ (b), and of the image contrast (c) measured for the Ar, Ko, and MW series. Legend as in Figure 2.

that time due to instrumental problems and undersized grating, respectively.

Stray-light level. We computed the median intensity over rings centered on $\mu = 1$ and evaluated the profile of these median values in each image, starting from the disk center up to the image edge. Each ring is 1 pixel thick. In order to compare the stray-light level in all series, we have then used these calculated radial profiles to evaluate the ratio of the intensity values at fixed off-limb distances (e.g., $r/R_\odot = 1.06 \pm 0.01, 1.125 \pm 0.025, 1.225 \pm 0.025$) to that at the disk center ($I/I(0)$ hereafter), i.e., the aureola intensity. Note that the analysis of

regions just outside the solar disk ($r/R_\odot$<1.3) is aimed to avoid the influence of strong intensity inhomogeneities often observed further away from the solar disk. These inhomogeneities are mostly due to unexposed plate regions, calibration exposures, and inscriptions on the original plate.

We found that historic Ar, Ko, and MW images are strongly affected by stray light, much more than modern Me and PSPT data (see Table 2). Moreover, we found that Me spectroheliograms suffer more from stray light than PSPT filtergrams. Of the historical data sets, Ko images display the lowest mean stray light. Changes in instrumental conditions and setups are well seen on the temporal variation of the measured stray-light level. For instance, Figure 3(b) shows a large reduction of the stray-light level for the MW data taken from 1960 onward, which is probably due to the installation of new gratings noted in the observatory logbooks. The obtained results also clearly show effects of the aging of both instruments and observing programs. In fact, the stray-light level increased with grating use, since that component degraded in the open air installation of the spectrograph.

Image contrast. We analyzed the center-to-limb variation of intensity values of quiet Sun regions (CLV hereafter). The CLV was evaluated on each image by computing the median of intensity values over each of 20 rings of equal area centered on the solar disk center. We also determined the intensity contrast, $(I_{\max} - I_{\min})/(I_{\max} + I_{\min})$, where $I_{\max}$ and $I_{\min}$ are the largest and the smallest values among the 20 intensity values thus determined. Note that the usage of the small number of rings and of the median intensity in each ring is aimed to lower the influence of image defects and of active regions on the obtained results.

We found that, on average, the contrast value measured for modern data is up to ≈50% lower than that resulted for historic series (Table 2). Moreover, the standard deviation of contrast measurements for modern data is about 10 times lower than that for historic data. This may partly be due to the larger samples of historic images covering longer periods of time. However, the main reason is probably the higher stray-light level and the uncertainties in the photographic calibration of the historic data. For instance, the method applied in this study to perform the photographic calibration makes use of pixel values of both unexposed and dark regions of the original plate, which might be poorly defined in the analyzed data. Changes in instrumentation and the observing procedure are also well seen in the temporal variation of the image contrast measured for the three historic series (Figure 3(c)). We found that the standard deviation of values measured over a year (Table 2), which takes into account seasonal variations of the image quality, instrumental changes, and occasional failures of the algorithms used for radii measurements, is close to the standard deviation of the annual averages (Table 3). Finally, comparison between Figure 3(c) and (b) shows that the temporal variations of stray-light level and of image contrast are anticorrelated for each series. This is not surprising given the effects of stray-light degradations on the CLV (Martìnez Pillet 1992).

3.2. Discussion

The difference between the image contrast of historic and modern observations found in Section 3.1 is particularly worrisome since this parameter lies at the heart of the scientific evaluation of the historic images. This difference may be caused by differences in spectral sampling (e.g., if historic and modern data were to sample different parts of the line profile), calibration issues, or degradations due to stray light.

Peculiarities in the spectral sampling of the historic data seem unlikely to be responsible for the difference in image contrast described in Section 3.1. In order to test this, we measured the relative difference between the CLV curves computed for K_3 and K_{1V} Me images recorded on average less than 2 minutes apart. We found that the dispersion of the CLV curves computed for the Me images obtained with the two spectral samplings in the same observing day is smaller than the dispersion of results obtained for spectrally homogeneous data taken on different days. In particular, the median value and the standard deviation of the relative difference between the CLV curves computed for the two samples of spectral images are -0.006 ± 0.016 for all disk positions with $\mu \geqslant 0.4$. The same quantities computed for the sample of K_3 images, with respect to a randomly selected K_3 image, are -0.003 ± 0.020. Similar results were obtained for a few Ca II K spectroheliograms taken recently at the Coimbra Observatory. In order to evaluate the effects of the photographic calibration on the results presented in Section 3.1, we analyzed images obtained by applying three different calibration methods to a given sample of MW observations. This sample consists of 713 observations taken in 1967 and 1975. The three methods are: (1) the one applied by the UCLA project scientists (UCLA hereafter), which takes into account the calibrated exposures available on the side of the solar observations; (2) the method described in Section 2.2 (*calib* hereafter); and (3) a method based on the assumption of a linear relation between the pixel values in the analyzed images and the incident flux (*linear* hereafter).

We found that the mean value of the image contrast measured on MW images varies by up to about 25% depending on the calibration method applied to the data. Moreover, the measured contrast changes by about 10% by modifying the numerical criteria used for the identification of the unexposed and the darkest pixels of the images in the *calib* method. In particular, the pixel identification was performed by using four sets of threshold values, which are based on: (1) maximum and minimum values of PV measured inside the solar disk; (2) maximum and minimum values of PV measured on the whole image; (3) higher than $m + 3\sigma$ and lower than $m - 3\sigma$, where m and σ are the mean and the standard deviation of PV measured inside the solar disk, respectively; and (4) constant values (32,767 and 0, respectively). The range of intensity values for quiet Sun regions obtained from the UCLA calibrated sample is smaller than that computed for the other two samples of images for all disk positions with $\mu > 0.25$, which corresponds to about 95% of the solar disk. The dispersion of CLV curves over 90% of the solar disk is about 25%, 33%, and 76% for the *linear*, *calib*, and UCLA image samples, respectively. In summary, the intensity CLV of quiet Sun regions computed for the UCLA calibrated sample is flatter than those obtained with the other two samples of data, but the dispersion of curves computed from 1 day to the next for the UCLA sample is larger than those for the other samples. Note that the values measured on all analyzed *calib* images approach those obtained from modern observations (Me and PSPT). However, the standard deviation of the values measured for *calib* historic images is about four times larger. In addition, the aureola intensity is considerably higher.

4. APPLICATION TO SOLAR ACTIVITY STUDIES

4.1. Contrasts and Plage Coverage in the Three Historic Time Series

Analysis of historic Ca II K observations is particularly interesting for investigations of solar activity and variability on timescales from the solar cycle to a century. For instance, it al-

lows the temporal range in which observed surface distributions of magnetic features enter models of solar irradiance variations (e.g., Krivova et al. 2003; Fontenla et al. 2004; Wenzler et al. 2005) to be extended. We now investigate the utility of the historic series for evaluation of solar activity variations. In particular, we analyze and compare the intensity distribution over the solar disk and the fraction of the solar disk occupied by bright features as a function of time for each series. Already visual inspection reveals considerable differences between the images from the three analyzed series taken on the same day. For example (Figure 1), the MW images show filaments over the solar disk, which are not found in the other data, although some are hinted at in the Ar images. On the other hand, Ko images show sunspots which are almost absent in the MW observations, and are partly found in the Ar data. Moreover, the position, dimension, and number of bright features seen in the images are quite different, especially close to the solar limb. The different observing time at the three sites, which may differ by more than 16 hr due to the site location, can explain part of these differences. However, the bulk of them arise from the different spectral sampling of these observations. In particular, observations taken with a narrow spectral sampling centered at K_3 show on-disk filaments, while those taken in a spectral range including $K_{1V,1R}$ show sunspots. Other problems of and differences between the three series area described in Section 3. Thus, a detailed analysis and intercomparison of three different series is particularly important for filtering solar variations from systematic instrumental problems, differences or changes.

After the processing described in Section 2.2, we have corrected the images for the center-to-limb variation of the quiet Sun intensity (CLV). We estimated the CLV on each image by computing the median intensity value on 100 concentric constant area annuli of the solar disk. The set of computed intensities was used to create the surface representative of the CLV pattern. Each image was then divided by the corresponding CLV. Finally, the intensity scale was shifted such that quiet Sun values lie around zero. In the following we refer to these images as contrast images and to pixel contrast values as the pixel values on these images.

We found that the CLV computation based on this definition is robust with respect to image artifacts such as intensity inhomogeneities and emulsion scratches. However, most of the processed images continue to show large-scale contrast patterns which have the potential to strongly affect the results of our investigation. In order to compensate for these patterns, each row of the analyzed images was then divided by the quadratic profile which best fits the contrast values of quiet Sun regions along the considered row. Pixels belonging to active regions in each analyzed row were identified by applying a contrast threshold criterion and then discarded. The same procedure was subsequently applied also to each column of the analyzed images. We also applied other methods presented in the literature (Brandt & Steinegger 1998; Worden et al. 1998; Caccin et al. 1998; Zharkova et al. 2003), but found that the simple method described above compensated the large-scale contrast patterns affecting the analyzed images more efficiently.

We first investigated effects of using different photographic calibration methods on observations taken at different activity levels. To this end, we chose image pairs from MW and MW/UCLA available for 1964 (activity minimum) and 1968 (activity maximum). This sample contains 71 and 60 image pairs for the two years, respectively. These cover the minimum and the maximum of sunspot number for solar cycle 20. For each image

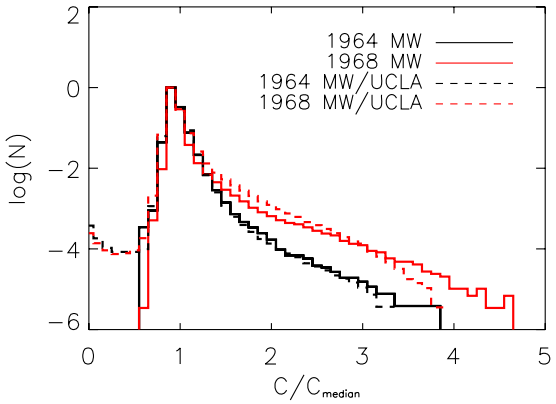

Figure 4. Histograms of the yearly median of pixel contrasts computed for the MW and MW/UCLA data sets. Details are given in Section 4.1. Each histogram is normalized to its maximum and shown in a lognormal plot to point out the differences between the computed distributions. All contrast values (C) were divided by the median contrast ($C_{\rm median}$) of the corresponding image.

(A color version of this figure is available in the online journal.)

of this sample, we computed the distribution of contrasts of individual pixels. We then evaluated the median distribution for each year. The produced histograms are shown in Figure 4 on a lognormal plot to better display the differences between the computed distributions.

We found that the distributions computed for the same year show a rather similar shape at intermediate contrast values irrespective of the calibration method. The first four moments of distributions are also similar. On the other hand, the tails of computed distributions clearly show the effects of different calibration methods on lower and higher contrast values on the solar disk. This is particularly clearly seen when comparing the distributions obtained for 1968 at the maximum of solar activity.

We then considered such median distributions for the years of sunspot number minima and maxima for cycles 17–20, i.e., the cycles covered by all three historic series. In this manner, we investigate how the data from the three time series compare to each other. All the data available for each year and series were employed to produce the distributions plotted in Figure 5 on lognormal axes. The number of analyzed images depends on both, the data set and the year. It varies from 45 (Ar, 1944) to 639 (MW, 1958).

The distributions computed for both Ko and MW series appear broader than those obtained for the Ar set (Figure 5). This is likely due to both the smaller number of available solar observations and the stronger image defects, namely, solar disk eccentricity, large-scale inhomogeneities, and stray light, affecting the Ar series with respect to the other sets. However, the moments of the distributions indicate that the compared populations of contrast values are rather similar. On the other hand, the shape of the distributions varies in time without a plain trend. This is especially clear when comparing the tails of distributions populated with lower or higher pixel contrast values. This likely results from changes of the spectral sampling of solar observations in each series with time. Nevertheless, the distribution obtained for 1958 is the broadest among all the distributions computed for each series.

Next, we analyzed the bright features on the images. In order to identify these features, we applied the method presented by Nesme-Ribes et al. (1996). This method makes use of a threshold value which is obtained for each image by studying the variation of the average of quiet Sun contrast for different thresholds.

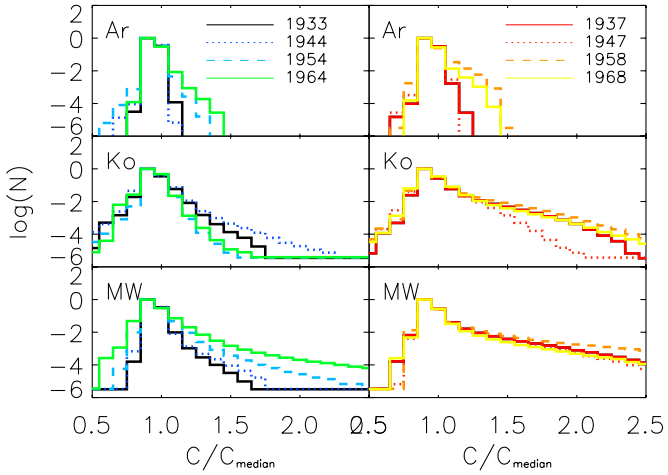

Figure 5. Histograms of the yearly median of pixel contrast distributions computed for the Ar, Ko, and MW time series. Results obtained from the three series for minimum (left panels) and maximum (right panels) years of solar cycles 17–20 are shown with different colors. Details are given in Section 4.1 and in the caption of Figure 4.

(A color version of this figure is available in the online journal.)

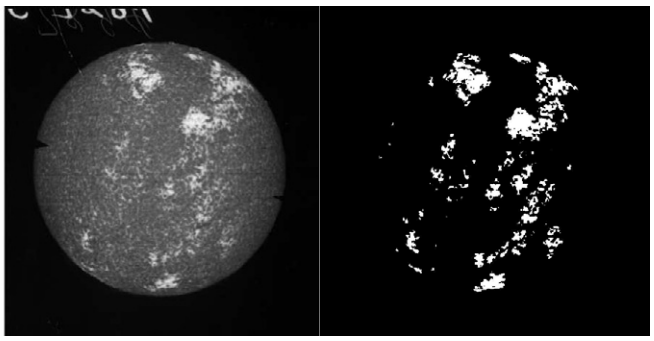

Figure 6. Sample images obtained by the processing described in Section 2.2 (left) and by the plage identification outlined in Section 4.1 (right). The original image was taken on 1958 June 22 (MW series.)

Thus, the identification criterion is based on objective results of image analysis. However, this method fails to discriminate bright features belonging to active regions (henceforth referred to as plage regions) from those occurring on the quiet Sun (network regions). Following Ermolli et al. (2007), we singled out these two classes of features by further taking into account continuity and size of features identified with the contrast thresholding (see Figure 6 for an example). The selection of only bright features belonging to active regions facilitated the comparison of our results with those available in the literature.

Finally, we computed the area, corrected for foreshortening, of each identified plage region. We then evaluated the fraction of the solar hemisphere covered by plage on each image (henceforth referred to as plage coverage) and evaluated their annual median values.

Figure 7 shows the temporal variation of the yearly median of the plage coverage obtained from the Ar, Ko, and MW series. The values obtained from the three data sets agree within 40%. The Pearson correlation coefficients are 0.87, 0.85, 0.93 for the pairs of Ko–MW, Ar–Ko, and Ar–MW, respectively. The mean of these values is 0.88. However, the plage coverage evaluated from the three series differs considerably for cycles 15, 17, and 19. The relative difference between the median values obtained for the three series is up to 140% in these cycles. These differences are not surprising given the findings of

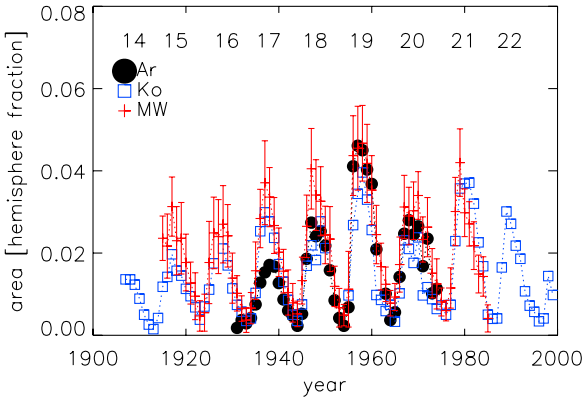

Figure 7. Temporal variation of yearly median values of the plage coverage measured from the Ar, Ko, and MW series. Details are given in Section 4.1. The error bars represent the standard deviation of measured values over the annual interval; for clarity, they are only shown for the MW series. Cycle numbers are given at the top of each cycle.

(A color version of this figure is available in the online journal.)

Section 3. In particular, we showed that both Ar and MW series suffer from strong large-scale inhomogeneities and stray-light degradations in the first decade of observations (solar cycles 15 and 17, respectively). If we exclude these data, the results, on average, agree within 25%. The mean of the Pearson correlation coefficients also increases to 0.92.

4.2. Discussion

The difference between the plage coverage obtained from the three analyzed historic series questions the reliability of solar activity models based on these data and calls for a detailed discussion of measurement errors. Assessment of these errors is hampered by several factors, e.g., differences and changes in the instruments used to obtain the original photographic observations, as well as in the digitization. Nevertheless, the uncertainties associated with the data processing applied in this study can steadily be investigated. The results obtained for the MW series can also be compared with those of Foukal (1996), who analyzed images produced by the first digitization of the MW Ca II K spectroheliograms. This digitization was performed with a commercial device, which produced images with a 512 × 512 format and 8 bit data significance. Plage coverage measurements obtained by Foukal (1996)[6] were derived by applying an interactive identification of features on linearly calibrated digital images.

Figure 8 compares yearly median plage coverage obtained by Foukal (1996) and in this work (MW series). We found that, on average, the two sets of area values lie within ≈10% of each other. The mean of the Pearson correlation coefficient computed for each cycle of the two sets is 0.95. However, the values obtained in this study are systematically lower than those obtained by Foukal (1996), in particular around the peak of solar cycle 19, when the values lie almost a factor of 2 apart. The median values of the two compared sets of measurements differ by up to ≈100% in this cycle.

Errors in the identification of features seem unlikely to be responsible for this difference. In order to test this, we processed the modern PSPT data applying the same scheme as for the historic sets and compared the results with those provided by an independent analysis of Ca II K present-day observations,

[6] Available through the NOAA/SDC archive at http://www.ngdc.noaa.gov/stp/SOLAR/ftpcalcium.html.

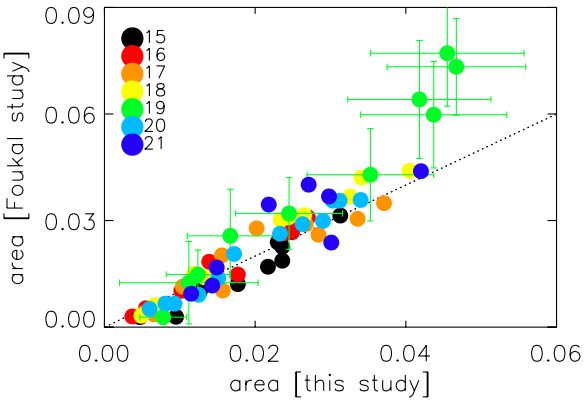

Figure 8. Yearly median plage coverage obtained by Foukal (1996) vs. plage coverage from the MW series. The different colors refer to solar cycles 15–21. The error bars represent the standard deviation of plage areas over a year; for clarity, error bars are plotted only for solar cycle 19. The dotted line indicates perfect agreement between the two sets.

(A color version of this figure is available in the online journal.)

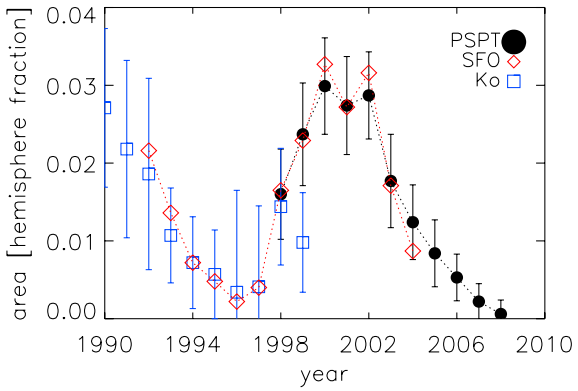

Figure 9. Temporal variation of the yearly median values of the facular coverage measured from the PSPT data set together with the variation of the corresponding quantities independently evaluated from the Ca II K observations taken the San Fernando Observatory (SFO). Details are given in Section 4.2. Also shown the temporal variation of the yearly median values of the facular coverage measured from the Ko series for 1990s. The error bars represent the standard deviation of facular areas measured over the annual interval.

(A color version of this figure is available in the online journal.)

specifically those taken and analyzed at the San Fernando Observatory (S. Walton 2005, private communication). The median values over annual intervals of the two sets are in good agreement (Figure 9) and the Pearson correlation coefficient is 0.99. In particular, the median and the standard deviation of values describing the relative difference between the two sets of measurements from 1998 to 2004 are 0.7% and 15%, respectively. The same quantities obtained for the Ko versus San Fernando series for 1990s are 1.5% and 22%, respectively, and the Pearson correlation coefficient is 0.99 (Figure 9). These results indicate that the identification criterion used in this study produces plage area measurements which are in agreement with those already used for the modeling of solar activity and variability (e.g., Walton et al. 2003; De Toma et al. 2004).

Finally, we have investigated the effect of the employed photographic calibration method on the results presented. For this, we have also identified plage regions on the same sample of images taken from 1961 to 1985, which were linearly calibrated (MW/*linear*, see Section 3.2) and calibrated by the UCLA team (MW/UCLA, see Section 2.1). These images cover solar cycles 19–21. We found that the annual median values of plage coverage from the MW and MW/UCLA samples agree, on average, within 3%, although in cycle 21 they differ by up to 40%. The Pearson correlation coefficient between the two sets is 0.92. At the same time, the annual median values of plage coverage from the MW/*linear* sample underestimate the values obtained for the MW/UCLA set, on average, up to 25%, although the Pearson correlation coefficient between the two sets is 0.97. These results suggest that application of a calibration method such as that used on MW/UCLA data to the three historic series would rather little affect the plage areas presented in Section 4.1. On the other hand, application of a linear calibration to MW observations would give even lower values and they would not allow us to produce the higher plage coverage as given by Foukal (1996).

5. CONCLUSIONS

We analyzed the image contents of three historic time series of Ca II K spectroheliograms obtained by the digitization of the Ar, Ko, and MW photographic archives. We measured the image contents trough several quantities and compared the obtained results with those deduced from similar present-day observations.

Perhaps unsurprisingly, our study shows that historic data suffer from stronger degradation effects associated with instrumental problems than similar modern observations. Some of the image problems described in this study, e.g., the disk eccentricity, can be fixed through application of an appropriate technique, e.g., the one we have presented. Some other problems, such as the photometric uncertainties associated with photographic calibration, stray light, and variation in time of image contents (e.g., produced by shifts in the wavelength of the observation), are more difficult to account for with image processing. In particular, the temporal variations of the image contents due to instrumental changes can be separated out from solar temporal variations only through the intercomparison of the data from different archives. Our results suggest that for such intercomparison it would be extremely useful to digitize the Ko series with a higher quality than available at present, since the Ko series turns out to be both the most homogeneous and longest among those considered.

The segmentation technique tested in this study, which was developed to single out plage regions on present-day Ca II K observations, provided reasonably consistent results for the three series, after they were processed with photographic calibration methods used in the literature. Although there are some differences in the fraction of the solar hemisphere covered by plage regions as evaluated for the three series, the difference to the result of Foukal (1996) is larger, in particular around the peak of solar cycle 19. This shows that caution is needed when using such data in variability models (e.g., Crouch et al. 2008) without careful analysis of their problems and intrinsic instrumental variations.

This study represents a first step toward a careful and systematic exploitation of the resource of historic Ca II K time series, but considerable further work remains to be done before they can be widely employed for reliably deducing long-term solar activity and variability.

This study represents a first step toward a careful ad systematic exploitation of the resource of historic Ca II K time series, but considerable further work remains to be done before they can be widely employed for reliably deducing long-term solar activity and variability. Meanwhile, other studies have been

carried out that analyze some series presented here (Ermolli et al. 2007, 2009; Criscuoli & Ermolli 2008; Foukal et al. 2009; Tlatov et al. 2009). The discussion of results obtained by all these studies will be presented in a forthcoming paper.

The authors thank the Arcetri, Kodaikanal, Meudon, Mt Wilson, and the Rome Solar Groups, A. Garcia and the late S. Walton for the data provided. J. Aboudarham, F. Cavallini, and J. M. Malherbe are acknowledged for useful discussions. This work was partly supported by the CVS project (Regione Lazio) and by the Deutsche Forschungsgemeinshaft, DFG project SO-711/1-2. The digitization of the Mt Wilson Photographic Archive has been supported by the US National Science Foundation grant ATM/ST 0236682.

REFERENCES

Acton, L., et al. 1992, Science, 258, 618
Bappu, M. K. V. 1967, Sol. Phys., 1, 151
Brandt, P., & Steinegger, M. 1998, Sol. Phys., 177, 287
Caccin, B., Ermolli, I., Fofi, M., & Sambuco, A. M. 1998, Sol. Phys., 177, 295
Centrone, M., Ermolli, I., & Giorgi, F. 2005, Mem. Soc. Astron. Ital., 76, 941
Chapman, G. A., Cookson, A. M., Dobias, J. J., Preminger, D. G., & Walton, S. R. 2004, Adv. Space Res., 34, 262
Coulter, R. L., & Kuhn, J. F. 1994, in ASP Conf. Ser. 68, Solar Active Region Evolution: Comparing Models with Observations, ed. K. S. Balasubramaniam & G. W. Simon (San Francisco, CA: ASP), 37
Criscuoli, S., & Ermolli, I. 2008, A&A, 484, 591
Crouch, A. D., Charbonneau, P., Beaubien, G., & Paquin-Ricard, D. 2008, ApJ, 677, 723
Dainty, J. C., & Shaw, R. 1974, Image Science (New York: Academic)
Delaboudinière, J.-P., et al. 1995, Sol. Phys., 162, 291
Denker, C., Johannesson, A., Marquette, W., Goode, P. R., Wang, H., & Zirin, H. 1999, Sol. Phys., 184, 87
Deslandres, H. 1891, C. R. Acad. Sci. Paris, 131, 307
Deslandres, H., & D'Azambuja, L. 1913, C. R. Acad. Sci. Paris, 157, 413
De Toma, G., White, O. R., Chapman, G. A., Walton, S. R., Preminger, D. G., & Cookson, A. M. 2004, ApJ, 609, 1140
de Vaucouleurs, G. 1968, Appl. Opt., 7, 1513
Ellerman, F. 1919, PASP, 31, 16
Ermolli, I., Berrilli, F., & Florio, A. 2003, A&A, 412, 857
Ermolli, I., Criscuoli, S., Centrone, M., Giorgi, F., & Penza, V. 2007, A&A, 465, 305
Ermolli, I., Fofi, M., Bernacchia, C., Berrilli, F., Caccin, B., Egidi, A., & Florio, A. 1998, Sol. Phys., 177, 1
Ermolli, I., Marchei, E., Centrone, M., Criscuoli, S., Giorgi, F., & Perna, C. 2009, A&A, preprint doi http://dx.doi.org/10.1051/0004-6361/200811406
Ermolli, I., Tlatov, A. G., Solanki, S. K., Krivova, N. A., & Singh, J. 2007, in ASP Conf. Ser. 368, The Physics of Chromospheric Plasmas, ed. P. Heinzel, I. Dorotovic, & R. J. Rutten (San Francisco, CA: ASP), 533
Evershed, W. 1911, MNRAS, 71, 719
Fontenla, J. M., Harder, J., Rottman, G., Woods, T. N., Lawrence, G. M., & Davis, S. 2004, ApJ, 605, L85
Foukal, P. 1996, Geophys. Res. Lett., 23, 16, 2169
Foukal, P., Bertello, L., Livingston, W. C., Pevtsov, A. A., Singh, J., Tlatov, A. G., & Ulrich, R. K. 2009, Sol. Phys., 255, 229
Fuller, N., Aboudarham, J., & Bentley, R. D. 2005, Sol. Phys., 227, 61
Gasperini, A., Mazzoni, M., & Righini, A. 2004, G. Astron., 3, 23
Giorgi, F., Ermolli, I., Centrone, M., & Marchei, E. 2005, Mem. Soc. Astron. Ital., 76, 977
Godoli, G., & Righini, A. 1950, Mem. Soc. Astron. Ital., 21, 4
Kariyappa, R., & Pap, J. M. 1996, Sol. Phys., 167, 115
Keller, C. U., Harvey, J. W., & The Solis Team 2003 , in ASP Conf. Ser. 307, Solar Polarization, ed. J. Trujillo-Bueno & J. Sanchez Almeida (San Francisco, CA: ASP), 13
Krivova, N. A., Solanki, S. K., Fligge, M., & Unruh, Y. C. 2003, A&A, 339, L1
Lefebvre, S., et al. 2005, Mem. Soc. Astron. Ital., 76, 862
Makarov, V. I., Tlatov, A. G., Singh, J., & Gupta, S. S. 2004, in IAU Symp. 223, Multi-Wavelength Investigations of Solar Activity, ed. A. V. Stepanov, E. E. Benevolenskaya, & A. G. Kosovichev (Dordrecht: Kluwer), 125
Marchei, E., Ermolli, I., Centrone, M., Giorgi, F., & Perna, C. 2006, Mem. Soc. Astron. Ital. S., 9, 51
Martìnez Pillet, V. 1992, Sol. Phys., 140, 207
Mickaelian, A. M., et al. 2007, A&A, 464, 1177
Mouradian, Z., & Garcia, A. 2007, in ASP Conf. Ser. 368, The Physics of Chromospheric Plasmas, ed. P. Heinzel, I. Dorotovic, & R. J. Rutten (San Francisco, CA: ASP), 3
Nesme-Ribes, E., Meunier, N., & Collin, B. 1996, A&A, 308, 2213
Ribes, E., & Mein, P. 1985, High Resolution in Solar Physics (Berlin: Springer)
Scherrer, P. H., et al. 1995, Sol. Phys., 162, 129
Schrijver, C. J., Coté, J., Zwaan, C., & Saar, S. H. 1989, ApJ, 337, 964
Skumanich, A., Smythe, C., & Frazier, E. N. 1975, ApJ, 200, 747
Tlatov, A. G., Pevtsov, A. A., & Singh, J. 2009, Sol. Phys., 255, 239
Ulrich, R. K., Webster, L. S., Varadi, F., Javaraiah, J., Lefebvre, S., & Gilman, P. 2004, AGU Fall Meeting Abstracts, SH52A-03
Walton, S. R., Chapman, G. A., Cookson, A. M., Dobias, J. J., & Preminger, D. G. 1998, Sol. Phys., 179, 31
Walton, S. R., Preminger, D. G., & Chapman, G. A. 2003, ApJ, 590, 1088
Wenzler, Th., Solanki, S. K., Krivova, N. A., & Fröhlich, C. 2005, A&A, 432, 1057
Worden, J. R., White, O. R., & Woods, T. N. 1998, ApJ, 496, 998
Zharkova, V. V., Ipson, S. S., Zharkov, S. I., Benkhalil, A. K., Aboudarham, J., & Bentley, R. D. 2003, Sol. Phys., 214, 89